

Article

# Continuously Tracking the Annual Changes of the Hengsha and Changxing Islands at the Yangtze River Estuary from 1987 to 2016 Using Landsat Imagery

Nan Xu <sup>1</sup>, Dongzhen Jia <sup>2,\*</sup>, Lei Ding <sup>3</sup> and Yan Wu <sup>4</sup>

<sup>1</sup> Ministry of Education Key Laboratory for Earth System Modelling, Department of Earth System Science, Tsinghua University, Beijing 100084, China; hhuxunan@gmail.com

<sup>2</sup> School of Earth Science and Engineering, Hohai University, Nanjing 211100, China

<sup>3</sup> Nanjing Hydraulic Research Institute, Key Laboratory of Port, Waterway and Sedimentation Engineering of the Ministry of Transport, Nanjing 210029, China; ld Ding@nhri.cn

<sup>4</sup> Shanghai Dahua Surveying & Mapping Co., Ltd., Shanghai 200136, China; 15951701953@163.com

\* Correspondence: jdz@hhu.edu.cn; Tel.: +86-133-9091-4608

Received: 5 December 2017; Accepted: 2 February 2018; Published: 8 February 2018

**Abstract:** The evolution of estuarine islands is potentially controlled by sediment discharge, tidal currents, sea level rise, and intensive human activities. An understanding of the spatial and temporal changes of estuarine islands is needed for environmental change monitoring and assessment in estuarine and coastal areas. Such information can also help us better understand how estuarine islands respond to sea level rise in the context of global warming. The temporal changes of two estuarine islands in Shanghai near the Yangtze River Estuary were obtained using Landsat TM (Thematic Mapper) and ETM+ (Enhanced Thematic Mapper) images from 1987 to 2016 on an annual scale. First, a composite image was generated by using the multi-temporal Landsat images for each year. Then, a modified normalized difference water index (MNDWI) was applied to the annual estuarine island maps using a threshold segmentation method. Finally, we obtained the temporal changes of the estuarine islands in Shanghai during the period 1987–2016. The results suggest that (1) Landsat TM/ETM+ images can be used for estuarine island mapping and change detection; (2) the two estuarine islands have expanded significantly during the past three decades; (3) human activities are the main driving factor that caused the expansion of the estuarine islands; and (4) the sea level can also partly explain the change in the estuarine islands. This study demonstrates that Landsat data are useful for determining the annual variations in the land area of two estuarine islands in Shanghai during the past 30 years. In the future, other factors and their contributions to estuarine island changes should be further investigated.

**Keywords:** estuarine islands; Yangtze River Estuary; Landsat data; remote sensing; Shanghai

## 1. Introduction

The evolution of estuarine islands can be shaped by sediment discharge, sea level rise, and tidal currents [1,2]. Intensive human activities near coastal areas can greatly change the morphologies of estuarine islands by the process of land reclamation [3–5]. Such coastal projects are common in coastal zones, particularly in coastal China, which has experienced rapid economic development since China's economic reform and opening-up in 1978 [6–10]. As the Chinese economic center, Shanghai undoubtedly needs new space for further economic development in the future [11]. Changxing Island and Hengsha Island are the second and third largest islands in Shanghai, which serves port, coastal industry, high-end service, and tourism functions. Because of intensive human activities around the two islands [12], timely and accurate information on the temporal changes of estuarine islands is

essential for deepening our understanding of how the coastal zone is changing and evaluating the impact of human activities. This information can also be used as the basis for sustainable development and environmental protection for Changxing Island and Hengsha Island. Therefore, it is important to track the coastline dynamic of these islands over long time periods.

To date, various remotely sensed data have been widely used for mapping and detecting changes in coastal zones because of their relatively low cost compared with traditional approaches [13–17]. In this study, Landsat imagery with a 30-m spatial and 16-d temporal resolution was selected as the main data source for tracking the temporal change of estuarine islands [18]. Unlike previous studies [19–22], this study aims to obtain an annual map of the estuarine islands and track their temporal changes at an annual scale rather than an interval of several years, which can provide more temporally detailed information on the estuarine islands' variations. Conventional methods that map changes in the estuarine islands over several-year intervals cannot detect more short-term changes [23]. Such changes are better characterized, with many observations using the method that was developed in this study. In addition, many coastline indicators have been proposed in previous studies [24]. For each year, Landsat time series images were firstly stacked together to generate a median image [25] after the removal of clouds and shadows. Based on the annual median image, the waterline [26] as the boundary between the estuarine islands and the surrounding water was then defined as the coastline on an annual scale. Finally, the annual land area of the estuarine islands was extracted from the annual median image.

The main objective of this study was to continuously track the dynamics of Changxing Island and Hengsha Island from 1987 to 2016 using a 30-m Landsat 4/5 Thematic Mapper (TM) and Landsat-7 (EMT+) Top of Atmosphere (TOA) reflectance product with the Google Earth Engine (GEE) [27]. Then, annual maps of the two estuarine islands were produced. Based on the generated data, a comprehensive description of the annual variations of the estuarine islands was presented, and the impact of human activities was investigated.

## 2. Study Area and Data

### 2.1. Study Area

The study area included Changxing Island and Hengsha Island, which are located near the Yangtze Estuary (Figure 1). Both islands were formed by sedimentation from the Yangtze River (also known as the Changjiang River), which, at 6380 km long, is the longest river in Asia and the third longest river in the world. The Yangtze runs west to east from the Anhui Province to the Jiangsu Province and finally flows into the East China Sea at Shanghai. The annual mean water discharge and sediment discharge of the river are  $905.1 \times 10^9 \text{ m}^3/\text{year}$  and  $0.43 \times 10^9 \text{ ton}/\text{year}$  during 1950–2000 [28]. The Yangtze River Estuary is characterized as a mesotidal estuary in terms of tidal range [29]. Tides are regular semidiurnal out of the mouth, and non-regular semi-diurnal inside. The mean (and maximum) tidal range is 2.66 m (4.62 m) at Zhongjun near the mouth, and decreases up-estuary to 2.43 m (3.96 m) at Gaoqiao and 2.21 m (4.48 m) at Wusong in the South Channel. In the background of climate change, the sea level around Shanghai has risen at a rate of 3 mm/year over the past three decades [30]. Since the construction of the Three Gorges Dam (TGD) in 2003, the suspended sediment discharge from the upstream into the estuary has been reduced from  $0.43 \times 10^9 \text{ ton}/\text{year}$  during 1950–2000 to less than  $0.15 \times 10^9 \text{ ton}/\text{year}$  up to now [28].

Shanghai, which features a humid subtropical climate with a mean annual air temperature of 17.1 °C and a mean annual precipitation of 1166.1 mm, is located in the Yangtze River Delta. The largest island in Shanghai, Chongming is an alluvial island at the mouth of the Yangtze River in eastern China, and it was 1267 km<sup>2</sup> in 2010. Combined with the Changxing and Hengsha Islands, it forms Chongming County, the northernmost area of the provincial-level municipality of Shanghai. The islands Changxing and Hengsha are the second and third largest islands in Shanghai. Changxing Island lies between Chongming and Shanghai in the southern channel of the Yangtze opposite to the

mouth of the Huangpu, the major river of central Shanghai. Hengsha Island lies in Changxing's east and is connected to the mainland and other islands. Changxing Island first emerged from the Yangtze in 1644, and it began to be reclaimed for agricultural purposes in 1843. Hengsha Island first emerged from the Yangtze in 1858, and it began to be reclaimed for agricultural purposes in 1886. Now, both Changxing Island and Hengsha Island are inhabited islands with developed agricultural, freshwater fishing, and marine fishing industries.

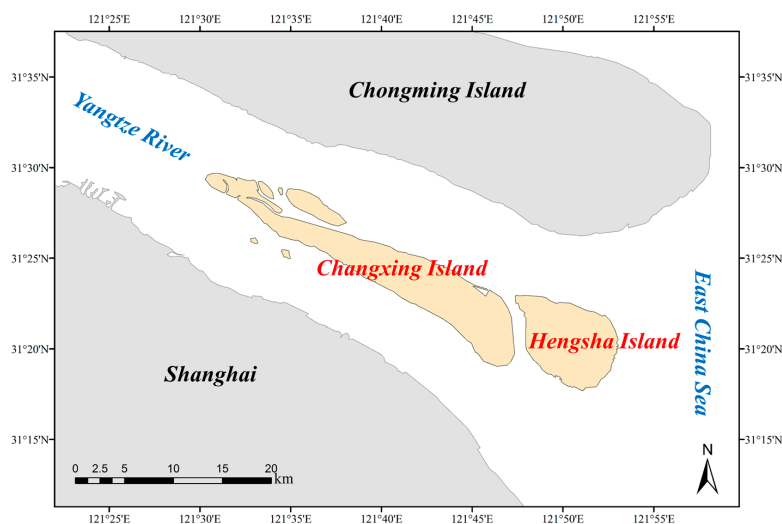


**Figure 1.** Geographical location of Changxing Island and Hengsha Island, Shanghai, China.

## 2.2. Data

To study the temporal changes of the two estuarine islands, time series of Landsat TM (Thematic Mapper) and ETM+ (Enhanced Thematic Mapper) Top of Atmosphere (TOA) reflectance data from 1987 to 2016 was used based on Google Earth Engine cloud platform. The spatial resolution of Landsat TM/ETM+ images is 30 m and the temporal resolution is 16 days. The study area was covered by the satellite track of path 118 and row 38. A total of 323 standard Level 1 Terrain-corrected (L1T) products were acquired for this scene. Specifically, 123 TM images during 1987–1999 and 200 ETM+ images during 2000–2016 were used. The annual distribution of the Landsat imagery and the annual percentage of cloud cover of the Landsat imagery were presented in Figure 2a,b, respectively. The number of Landsat images during 1987–2016 varies from 4 to 17 with no significant trend ( $R^2 = 0.0068$ ,  $p$ -value = 0.67). Also, the cloud cover during 1987–2016 varies from 4 to 17 with no significant trend ( $R^2 = 0.0078$ ,  $p$ -value = 0.64) in the cloud cover was found from 1987 to 2016.

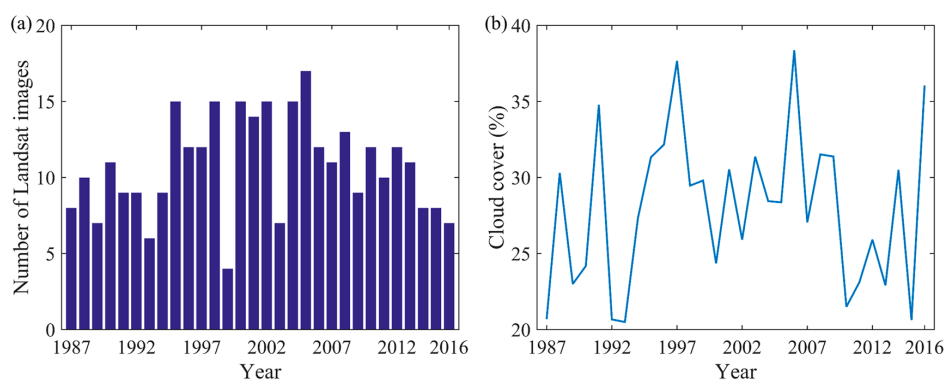


**Figure 2.** Detail information on the Landsat imagery used in this study. (a) The annual distribution of the Landsat imagery; (b) The annual percentage of cloud cover of the Landsat imagery.

### 3. Methods

GEE combines a multi-petabyte catalog of satellite imagery and geospatial datasets with planetary-scale analysis capabilities. Top of Atmosphere (TOA) calibrated Landsat 5 (TM) and 7 (ETM+) reflectance data that are available from the GEE platform were used for this study. A simple cloud score function (i.e., `ee.Algorithms.Landsat.simpleCloudScore()`) was used to avoid the influence of clouds and shadows on the Landsat data. A reduction function (i.e., `imageCollection.reduce()`) provided by GEE was applied to generate the annual Landsat time series from 1987 to 2016. For each pixel, the output is composed of the median value of all the Landsat images within each year at that location, which can effectively remove the noise caused by outliers and poorly removed edges of clouds [25]. For estuarine islands mapping, such median-composing method can minimize the short-term coastal changes associated with sea level variabilities, wave run-up, sedimentary seasonal variations, and coastal storms [18]. Note that the pixels in the Landsat 7 SLC-off gaps were not included in the generation of the annual Landsat images owing to their non-value characteristics. It means that the pixels contaminated by clouds, shadows, and Landsat 7 SLC-off gaps were not used for the calculation.

All annual Landsat images were generated based on GEE platform. The following operations performed for these downloaded annual Landsat images based on MATLAB are described below.

A land-water classification was the basic step that was performed during the estuarine island area extraction. The MNDWI has been widely used for land-water classification [31–34], and it was used in this study.

$$\text{MNDWI} = ((\text{Green} - \text{MIR})) / ((\text{Green} + \text{MIR})) \quad (1)$$

in which MIR is a middle infrared band (band 5 for Landsat TM/ETM+ data) and Green is the green band (band 2 for Landsat TM/ETM+ data).

The MNDWI was designed to enhance water features by composing various bands from multi-spectral remote sensing images. Based on the annual MNDWI image, a threshold segmentation method was performed to separate the land and water. For this process, it was critical to determine the threshold for the MNDWI image [35,36]. The frequency distribution of the annual MNDWI image was then counted. A 5-point moving average filter was applied to reduce the noise of the frequency distribution. The distribution formed two peaks, which represent the land and water around the estuarine islands. The threshold corresponding to the valley between the two peaks was determined and applied as the optimal threshold to separate the land and water (Figure 3). This method has a high effectiveness for land-water classification because of the significant spectral difference between the land and water areas. The MATLAB function “`imclose`” was used to avoid the spatial discontinuity of the land area around the boundary between the land and water in some regions. This function performs a closing operation with a structuring element. In this study, a square structuring element whose kernel size is 9 pixels was used in the experiments (Figure 4c). The MATLAB function “`imfill`” was applied to automatically fill the inland water of the estuarine islands in each land-water classification map (Figure 4d). This function fills holes in the input binary image (i.e., land represents 1 and water represent 0). The inland waters proposed herein were treated as land, since they are disconnected from the ocean. Finally, a 30-m resolution dataset of the multi-year estuarine island areas was generated for further calculations. Note that the TM images from 1987 to 1999 and the ETM+ images from 2000 to 2016 were utilized for this study because of data availability.

Annual maps of the two estuarine islands from 1987 to 2016 were obtained using the above-mentioned method based on GEE and MATLAB. To quantitatively investigate the temporal changes, the island area was selected as an indicator to characterize the temporal change of an island, as it is a fundamental property of an island. Specifically, annual area time series for each estuarine island and the combined total of the islands were calculated. For each island and the total, a linear regression model was adopted to estimate the long-term change rates of the land area variations. To further assess the temporal changes during different sub-periods, we visually divided the total

study period into several intervals based on the annual area time series. Two types of tipping points were considered in this study. The first one is the jumps in annual estuarine islands area. The second one is the jumps in the first-order derivative of annual estuarine islands area, which was used to represent the trend change in annual estuarine islands area. For each sub-period, the linear regression method was employed to investigate and analyze the rate of change in land area of each estuarine island and the total. The  $R^2$  and  $p$ -value for each linear regression were also computed.

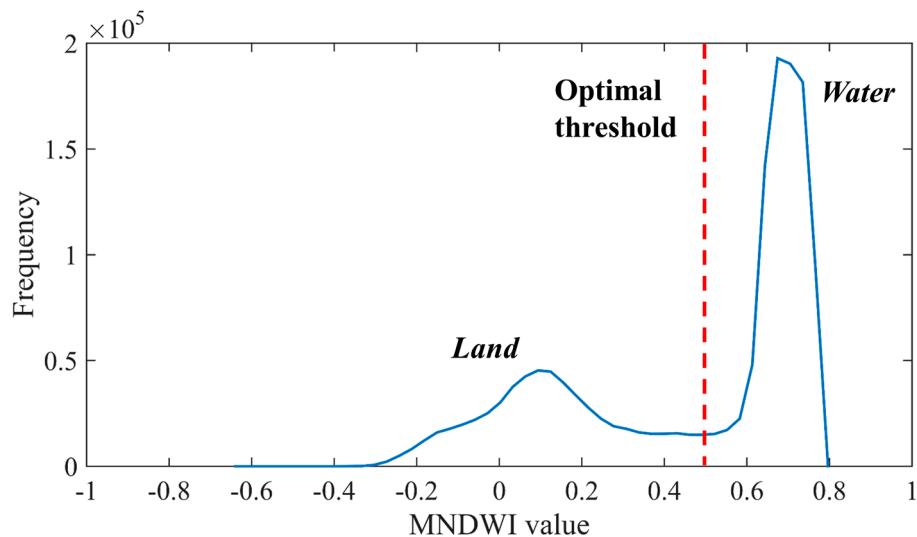


**Figure 3.** An example of determining an optimal threshold from the frequency distribution of an annual MNDWI map of the estuarine islands in 1990. Note that the frequency distribution has been smoothed with a 5-point moving average filter. The threshold corresponds to the valley of the MNDWI frequency distribution was determined as the optimal threshold.

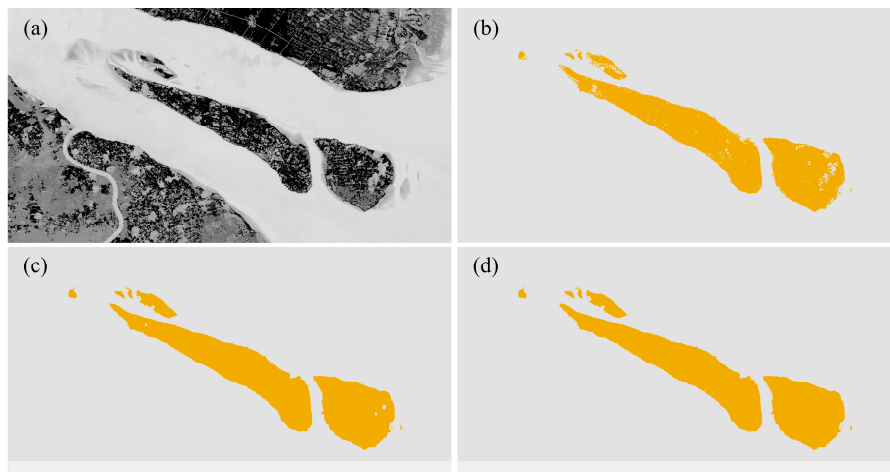


**Figure 4.** An example of generating an annual map of the estuarine islands in 1990. (a) The MNDWI image from 1990; (b) Land-water classification map after the thresholding segmentation; (c) Land-water classification map after the closing operation; (d) Land-water classification map after the filling operation (i.e., the final results); In (b–d), the yellow area represents the estuarine islands. In a, the light area represents the water body, and the dark area represents the land area.

## 4. Results

### 4.1. Estuarine Island Area Extraction

The estuarine island mapping results were produced from the MNDWI images. Figure 5 shows the extracted estuarine islands (including Changxing Island and Hengsha Island) for each year in the period from 1987 to 2016. In this figure, the background is the areas observed as permanent ocean area during 1987–2016. For each sub image in Figure 6, yellow and blue represent the dynamic ocean area and estuarine islands area for each year. Figure 6 demonstrates the annual variations in the areas of Changxing Island (blue line), Hengsha Island (yellow line), and the total (red line) from 1987 to 2016. The average, maximum, and minimum total areas were 226.6 km<sup>2</sup>, 283.5 km<sup>2</sup> (in 1990), and 181.2 km<sup>2</sup> (in 2015), respectively. The average, maximum, and minimum area of Changxing Island were 150.5 km<sup>2</sup>, 193.0 km<sup>2</sup> (in 1990), and 114.6 km<sup>2</sup> (in 2015), respectively. The average, maximum, and minimum area of Hengsha Island were 76.1 km<sup>2</sup>, 90.5 km<sup>2</sup> (in 1990), and 66.6 km<sup>2</sup> (in 2015), respectively.

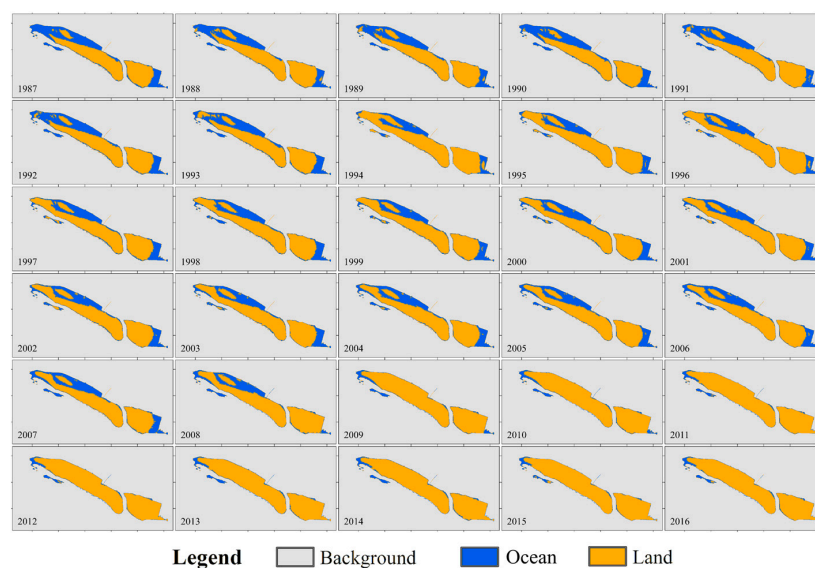


**Figure 5.** Spatio-temporal distributions of the estuarine islands from 1987 to 2016 with a 30-m spatial resolution and an annual scale, which show the expansion of Changxing Island and Hengsha Island. The yellow color represents land, and the blue color represents ocean. Note that land-ocean maps were limited in the area of land and dynamics ocean area. Background represents the permanent ocean area.

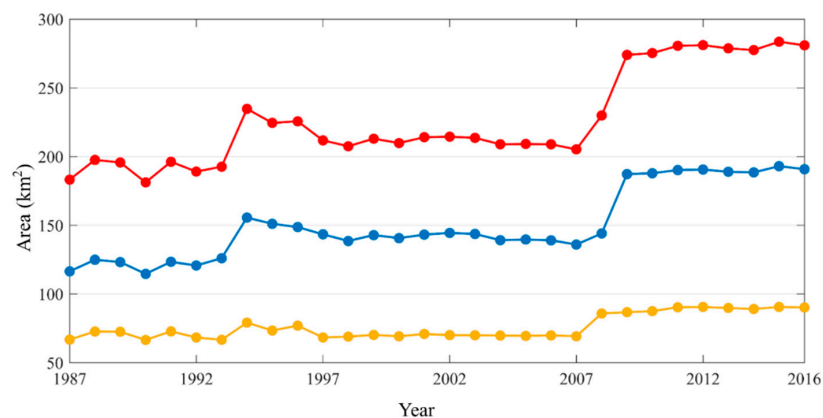


**Figure 6.** Annual variations in the areas of Changxing Island (blue line), Hengsha Island (yellow line), and the total combined island area (red line) from 1987 to 2016.

The spatial distribution of the frequency observed as land data in the period of 1987–2016 was used to characterize the spatiotemporal pattern of the estuarine island areas (Figure 7). The center of the estuarine islands had land frequency values close to 30, which signify permanent land coverage with a higher elevation. The areas with major variations, which had land frequency values between 0 and 30, were found in the northwest region of Changxing Island and the eastern region of Hengsha Island. Some variations were also observed around the western region of Changxing Island. The area that was observed to be land 100% of the time was 173.5 km<sup>2</sup>, or 57.6% of the entirety of the estuarine islands. Over the last three decades, a significant expansion (97.7 km<sup>2</sup>) of the estuarine islands’ land has occurred, and the majority of the land expansion occurred in the northern region of Changxing Island and the eastern region of Hengsha Island (Figure 8). The total change in these two regions in 2007 and 2008 is 68.8 km<sup>2</sup>, accounting for 70.4% of the land expansion during the period of 1987–2016. Both Figures 5 and 6 suggest obvious regional differences in the temporal changes of the estuarine islands.

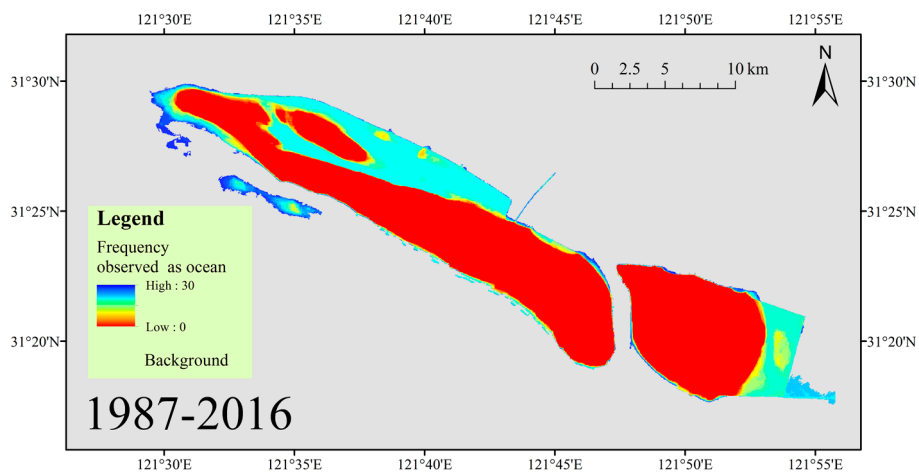


**Figure 7.** Spatial distribution of the frequency observed as ocean for the estuarine islands in the period of 1987–2016 with a resolution of 30 m. Background represents the permanent ocean area.

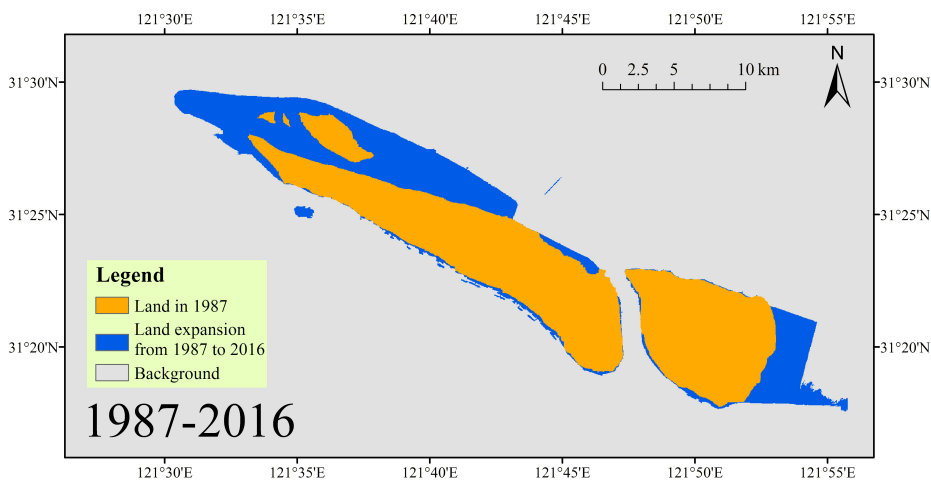


**Figure 8.** Change in the area of the estuarine islands between 1987 and 2016. The blue areas indicate land expansion from 1987 to 2016. Background represents the unchanged ocean area in 1987 and 2016.

4.2. Coastal Island Area Temporal Change

To quantitatively investigate the temporal changes of the estuarine islands, annual variations in the land areas of Changxing Island and Hengsha Island over the past 30 years are presented (Figure 9).

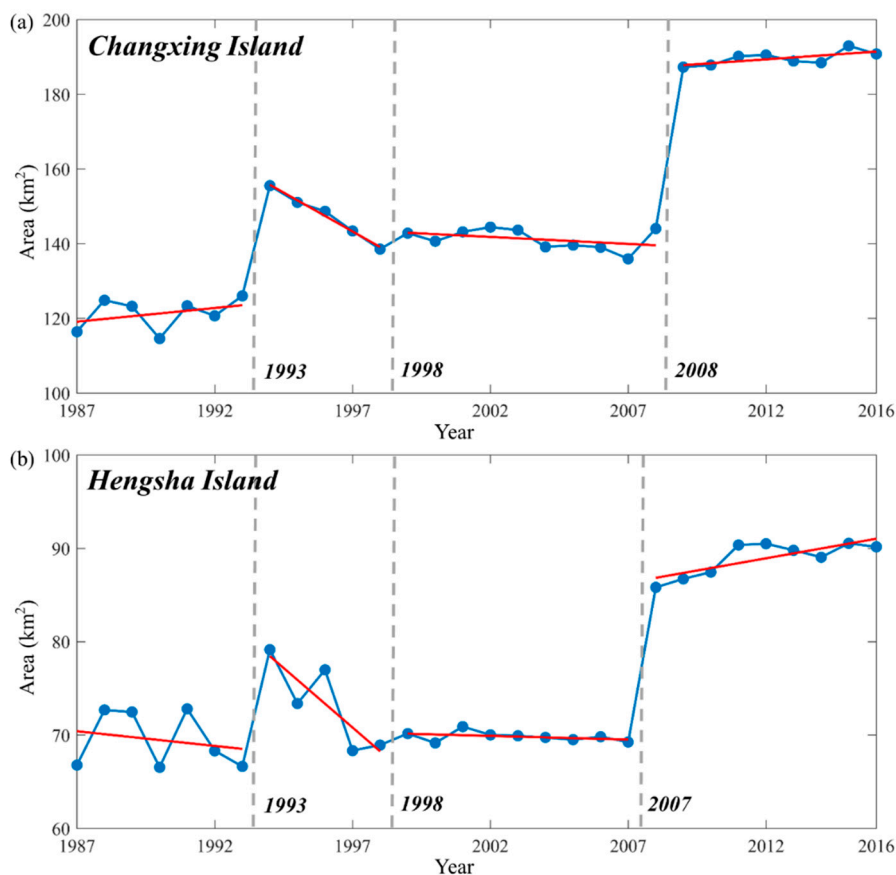


**Figure 9.** Annual variations in the land areas of (a) Changxing Island and (b) Hengsha Island during 1987–2016. The red line represents the linear regression line for each sub-period.

Our results suggest that both islands experienced a remarkable expansion during the study period despite sea level rise induced by climate change [30]. Changxing Island expanded from 116.4 km<sup>2</sup> to 190.8 km<sup>2</sup> with a net land increase of 74.3 km<sup>2</sup> and a change rate of 2.5 km<sup>2</sup>/year ( $R^2 = 0.73$ ,  $p$ -value < 0.001). Similarly, the area of Hengsha Island increased from 66.8 km<sup>2</sup> to 90.2 km<sup>2</sup> with a net land increase of 23.4 km<sup>2</sup> and a change rate of 0.8 km<sup>2</sup>/year ( $R^2 = 0.56$ ,  $p$ -value < 0.001). These statistically significant upward trends indicate that Changxing Island and Hengsha Island expanded during the last 30 years. In total, the area of the two islands increased from 183.2 km<sup>2</sup> to 280.9 km<sup>2</sup> with a change rate of 3.3 km<sup>2</sup>/year ( $R^2 = 0.71$ ,  $p$ -value < 0.001). Moreover, a certain amount of correlation in the annual variations of the two islands was observed ( $R^2 = 0.83$ ,  $p$ -value < 0.001), which reflects some consistency between the variations of the two estuarine islands.

Both Changxing Island and Hengsha Island show different variations at various time periods between 1986 and 2016 (Figure 9). To further uncover the characteristics of temporal change, the variations in the land area of the estuarine islands were divided into four sub-periods (1987–1992, 1993–1998, 1999–2008, and 2009–2016 for Changxing Island and 1987–1992, 1993–1998, 1999–2007, and 2008–2016 for Hengsha Island). The land area change rate and average value for each of the four sub-periods were calculated for each estuarine island (Figure 10). For Changxing Island, the change rates of the land area during four sub-periods were 0.7 km<sup>2</sup>/year, −4.2 km<sup>2</sup>/year, −0.4 km<sup>2</sup>/year, and 0.5 km<sup>2</sup>/year in temporal order. For Hengsha Island, the change rates of land area during the four sub-periods were −0.3 km<sup>2</sup>/year, −2.5 km<sup>2</sup>/year, −0.1 km<sup>2</sup>/year, and 0.5 km<sup>2</sup>/year in temporal order. In the first sub-period, the two islands displayed different change rates with slight variations. Both of the two islands exhibited significant land shrinkage during the second sub-period. In the third sub-period, both islands stayed at a relatively steady level and experienced slight land

shrinkage. A gradual land expansion was observed for the two estuarine islands in the last sub-period. Furthermore, we observed a declining trend in the land area of the estuarine islands in 2003 when the Three Gorges Dam (TGD) was put into operation (Figure 9).

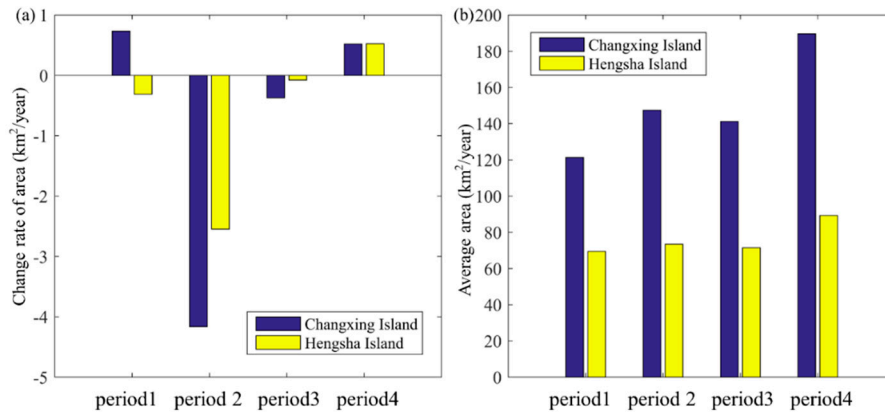


**Figure 10.** Change rates (a) and average values (b) of land area in Changxing Island and Hengsha Island during different sub-periods.

In addition, our results indicate some obvious sharp changes in the land area of the estuarine islands. Specifically, sharp changes in land area were observed in 1993 and 2008 for Changxing Island and in 1993 and 2007 for Hengsha Island (Figure 9). Including the significant land shrinkage of both islands that occurred during the second sub-period, land area change maps for the four sub-periods were produced (Figure 11). From 1993 to 1994, land expansion occurred in the northwest region of Changxing Island and the eastern region of Hengsha Island. From 1994 to 1998, considerable land shrinkage was observed in the eastern region of Hengsha Island, and slight land shrinkage was observed in the northwest region of Changxing Island. Combing the satellite images, the changes during 1993–1994 and 1994–1998 were natural and mainly controlled by the hydrodynamic conditions of the coastal regions. From 2007 to 2008, a significant land expansion was observed in the eastern region of Hengsha Island. From 2008 to 2009, a significant land expansion was observed in the northwestern region of Changxing Island.

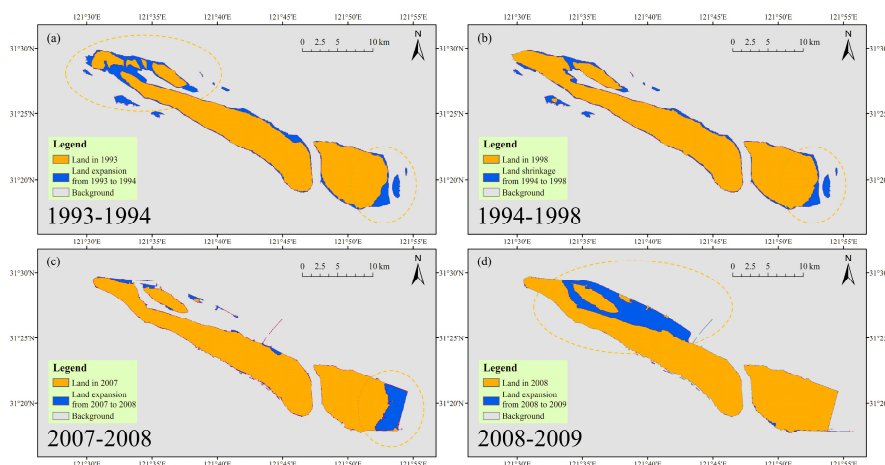


**Figure 11.** Dramatic changes of estuarine islands during four periods: (a) 1993–1994; (b) 1994–1998; (c) 2007–2008; and (d) 2008–2009. Regions within yellow ellipses well present the obvious change of estuarine islands. Background represents the unchanged ocean area during four periods.

Furthermore, Figure 12 displays the high-resolution images that are available on Google Earth, which clearly document the land reclamation in the coastal regions. The first row records the implementation of the Hengsha east shoal reclamation projects (phase III). These projects started in 2007 in order to provide a suitable location for a deepwater harbor site and new space for the development of Shanghai City [3]. Our results indicate that a land expansion of 16.56 km<sup>2</sup> occurred from 2008 to 2009, which is consistent with the area reported for these projects, 17.34 km<sup>2</sup>, in a previous study [37]. It is an example of land expansion induced by reclamations around the study areas during 1987–2016. The second row shows the Qingcaosha Reservoir, which is located at the lower reaches of the separation mouth of the south and north channels of the Changjiang River. To resolve water shortages in Shanghai, the Shanghai Municipal Government decided to build the Qingcaosha Reservoir as a water source in 2006 [38]. Subsequently, this project started construction in June 2007 and was put into operation in June 2011. The changes documented by the satellite images can be related to the human activities. Those changes tracked by high-resolution images agree with the results derived from the Landsat data, which could also be used as a validation of our proposed method of using Landsat data. The expansion of estuarine islands after execution of the Qingcaosha Reservoir is also consistent with the observed narrowing of the upper North Channel [29]. Specifically, a large part of the upper North Channel narrowed from 7.1 km to 4.3 km after the construction of levees.



**Figure 12.** High-resolution images from Google Earth that illustrate the sharp changes in land area that occurred in 2007 and 2008. The first row (a,b) and the second row (c,d) show the land reclamation in Hengsha Island and Changxing Island, respectively (regions within red ellipses).

Unlike many traditional methods for tracking estuarine islands at multi-decadal time scales, this study continuously monitored the temporal change of two estuarine islands with a yearly frequency, which can provide more temporally detailed information about estuarine islands variations. The traditional approach is simple to conduct but not always effective. One problem is that, during their moments of observation, corresponding images have to be at the same water level to minimize the impact of tidal inconsistencies. Another problem is that the images need to be obtained without clouds and shadows. Even under ideal conditions, only changes that occur between two images can be detected; it is difficult to capture changes that occur during the time between two images, which may be important. For instance, abrupt changes that occurred in 1993, 2007, and 2008 cannot be detected using conventional methods that use intervals of several years. Moreover, this method can avoid the effects of the Landsat 7 SLC (Scan Line Corrector)-off gaps caused by the failure of the Scan Line Corrector (SLC) in Landsat 7. Such method takes full advantage of all available pixels with good quality at a pixel level, while only Landsat images with a lower cloud percentage were used at a scene level in many conventional studies.

### 4.3. Influencing Factors Analysis

The results of the influencing factors analysis conducted on human activities, sediment discharge, and sea level are presented in Figure 13. In this study, the human activity mainly indicates the land reclamation in coastal zones around Hengsha Island and Changxing Island, which can directly reshape the coastline position of estuarine islands. Human activities, sediment discharge, and sea level data was collected from some previous studies [30,37,38]. Note that the annual estuarine islands change (i.e., first order difference of annual land area of estuarine islands) was used for analysis. Similar operations were conducted to sediment discharge and sea level data. Our results suggest that human activity is significantly correlated with the temporal change of coastline ( $R^2 = 0.41$ ,  $p$ -value < 0.001). During the past 30 years, land expansion caused by human activities is 85.72 km<sup>2</sup>, accounting for 87.73% of total land expansion of 97.71 km<sup>2</sup>. No significant relationship between annual sediment discharge and annual estuarine islands change was found ( $R^2 = 0.047$ ,  $p$ -value = 0.28). Also, no significant relationship between annual sea level and annual estuarine islands change was observed ( $R^2 = 0.011$ ,  $p$ -value = 0.59). The results suggest that no significant relationship between sediment discharge and estuarine islands change, sea level, and estuarine islands change was found at an annual scale during 1987–2016.

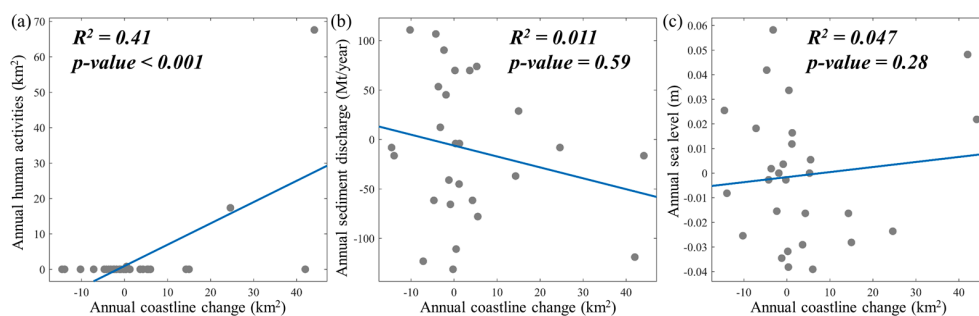


**Figure 13.** Influencing factors analysis. (a) Annual human activities; (b) Annual sediment discharge; (c) Annual sea level.

To further uncover the impact of sediment discharge and sea level on estuarine islands change, the same analysis was also conducted after removing the data with dramatic changes (i.e., 1993, 2007, and 2008). No significant relationship between annual sediment discharge and annual estuarine islands change was found ( $R^2 = 0.045$ ,  $p$ -value = 0.76) (Figure 14a). By contrast, a significant relationship between annual sea level and annual estuarine islands change was observed ( $R^2 = 0.114$ ,  $p$ -value < 0.01), which indicates a significant negative relationship (Figure 14b). After removing the data with dramatic changes, a significant increase of R-square between annual sea level and annual estuarine islands was found. However, no significant relationship between the sediment discharge and estuarine islands change was observed.

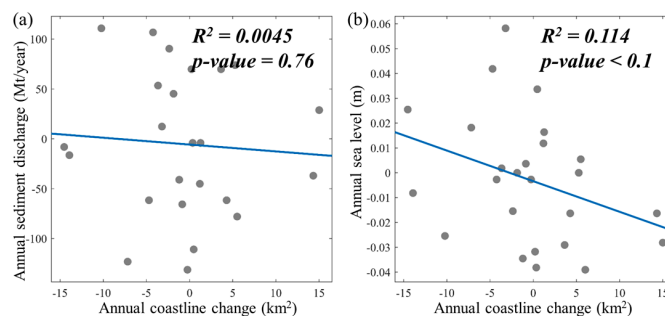


**Figure 14.** Influencing factors analysis after removing the data with dramatic changes. (a) Annual sediment discharge; (b) Annual sea level.

## 5. Discussions

### 5.1. Comparison of Results from Landsat TM/ETM+ Data

To test whether the results are sensitive to the selection of Landsat imagery, the annual land areas of Changxing Island and Hengsha Island were calculated from the TM data, and corresponding ETM+ data were obtained and compared. The time series during the 2000–2010 period with available Landsat TM and ETM+ data was used for comparison (red box in Figure 15). Two time series of the annual land area of Changxing Island (blue lines in Figure 15) exhibit good agreement ( $R^2 = 0.95$ ,  $p$ -value  $< 0.01$ ). Similarly, two time series of the annual land area of Hengsha Island (yellow lines in Figure 15) exhibit good agreement ( $R^2 = 0.92$ ,  $p$ -value  $< 0.01$ ). As shown in the inset of Figure 15, the annual land area of the entirety of Changxing Island and Hengsha Island also shows good agreement ( $R^2 = 0.99$ ,  $p$ -value  $< 0.01$ ). In general, good agreement is achieved between the annual variation of the land area of the estuarine islands derived from the TM and ETM+ data, which suggests that the Landsat imagery is able to characterize the annual variations of the estuarine islands' area. The comparisons confirm that the results are not sensitive to the selection of Landsat imagery.

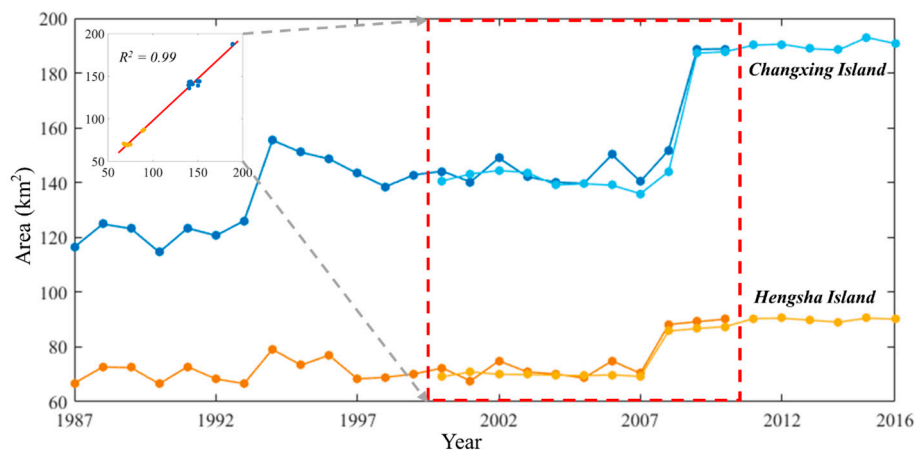


**Figure 15.** Different time series of the annual land area of Changxing Island and Hengsha Island derived from the TM and ETM+ data. The time series in the red box was used for the analysis. The inset figure shows the relationship between land areas derived from the TM and ETM+ data during the 2000–2010 period, which displays good agreement ( $R^2 = 0.99$ ,  $p$ -value  $< 0.001$ ).

In the future, accurate tidal levels during the Landsat observations can be collected to investigate the association between tidal level bias and island area. Furthermore, Landsat-8 Operational Land Imager (OLI) data can also be used for estuarine islands mapping, and Landsat TM, ETM+, and OLI images can be compared together.

### 5.2. Influencing Factors of Estuarine Islands Change

According to previous analysis in Section 4.3, expansion of estuarine islands during the past 30 years was significantly ( $R^2 = 0.41$ ,  $p$ -value  $< 0.001$ ) linked with the human activities (i.e., land reclamation). Based on previous studies, land reclamation in Changxing Island and Hengsha Island resulted in a great land expansion of 85.72 km<sup>2</sup>, accounting for 87.73% of total land expansion of 97.71 km<sup>2</sup> from 1987 to 2016. Additionally, high-resolution images from Google Earth also confirmed the sharp changes in land area that occurred in 2007 and 2008, which exhibited an agreement with previous studies [35]. Thus, we can conclude that human activities contributed to the great expansion of Changxing Island and Hengsha Island in the past 30 years. In the future, human activities can continuously result in the expansion of two estuarine islands according to the Shanghai's new strategic development plans [3].

Apart from human activities, natural factors such as sediment discharge and sea level were also potential factors of estuarine islands change. After removing the data with dramatic changes (i.e., 1993, 2007, and 2008), we explored the association between sediment discharge, sea level, and estuarine islands change. No significant relationship was found between estuarine islands change and sediment discharge ( $R^2 = 0.045$ ,  $p$ -value = 0.76). This means that the sediment discharge is not a dominant factor in the expansion of estuarine islands. Observations have confirmed a declining trend in sediment discharge during the past decades [30]. Li's study suggest that deposition occurred in the Yangtze River Estuary in the inshore area from a depth of 6.4 m after the construction of the TGD [39]. Significant erosion in the area below that water depth was observed until 2013. They concluded that the impoundment of TGD mainly controlled the evolution of topography around the Yangtze River Estuary. The observed nearshore deposition is mainly caused by coastal land reclamations. In reality, the Yangtze River Submerged Delta will undergo continuous erosion under sediment starvation induced by TGD and the construction of some other hydropower projects in the next decades.

Additionally, a significant negative relationship was observed between estuarine islands and sea level ( $R^2 = 0.114$ ,  $p$ -value < 0.01). The results show that the sea level variability can partly explain the estuarine islands change on an annual scale. Hence, we can conclude the human activities is the most important driving factor to temporal change of estuarine islands on an annual scale, which is consistent with the observations of Chen's study [40]. They found that the reclamation area increased with the decrease of barren mudflat and salt marsh around Shanghai. Besides, sea level can partly explain the change of estuarine islands. Furthermore, the significant negative relationship between sediment discharge and estuarine islands change suggests that the estuarine islands may face greater risk of erosion from future sea level rise.

The Yangtze River Submerged Delta will undergo continuous erosion under sediment reduction and sea level rise. In the future, the tidal flat in Shanghai will increase slowly and even decrease without protection. The coastline without levees will also advance to the ocean slowly and even retreat to the land. Consequently, it will retard the expansion of estuarine islands and even bring about the shrinkage of estuarine islands. Although human activities can significantly result in the expansion of estuarine islands, sediment discharge reduction and sea level rise are two potential factors associated with the erosion of estuarine islands. Hence, siltation promotion is needed to protect the wetland and land resource in coastal zones in the future.

In this study, we focused on the impact of sediment discharge and human activities on the Yangtze River Delta. However, some other estuarine processes, such as longshore currents, tidal currents, and wave currents, can also have potential influences on the estuarine islands change [41]. Liu et al. found that much sediment from the Yangtze River was transported southward by the longshore current along the inner shelf [42]. The tidal current on the flat is mainly back and forth along the river and gyrotory on the seaward side of the estuarine islands. The flow velocity on the intertidal flat gradually decreased when the elevation increased. The river discharge can enhance ebb flows and change current asymmetry, especially on the lower flat in neap tide, although hydrodynamics over the study area is tide-dominated [43]. The ebb tide, together with the longshore current, can carry about half of the sediment from the Yangtze River [44]. The wave current is another essential factor for the sedimentation in intertidal flat [43]. In subtidal area of the Yangtze River Estuary, wave climate was found dominated by waves generated by local winds. Such wind-induced wave current can result in short-term erosion-accretion processes because of the monsoon climate. In the future, these influencing factors can be quantified and the association between the longshore currents, tidal currents, wave currents, the estuarine islands change can be explored.

Note that although two driving factors of estuarine islands change have been identified, a sharp land expansion in 1994 remains unclear. From Figure 5, we can observe that some tidal channels changed from water to land in 1994 and some of them gradually became inundated by ocean in the next few years.

### 5.3. Further Considerations

A Landsat time series was used to map the estuarine islands and continuously track the temporal change of land area at an annual scale. A dataset of the yearly estuarine island maps that were produced in this study can be used to examine the impact of human activities on the evolution of estuarine islands. Owing to the limitation of spatial-temporal resolution of Landsat imagery, some spatial-temporal variabilities were undetectable. For the coastline of estuarine islands with a tiny change, a sub-pixel mapping technique may be needed to solve the spectral mixture problem of boundary pixels between the land and the ocean in estuarine islands mapping [45,46]. The monthly variations of the estuarine island areas can be captured by fusing multi-temporal MODIS (moderate-resolution imaging spectroradiometer) and Landsat data [47]. This dataset can support a better understanding of the seasonal variability of estuarine islands. Moreover, these data can be used to explore the response of estuarine islands to the occurrence of natural disasters (such as typhoons and tsunamis) around their coastal zones. Apart from the area, some other metrics, such as shape and centroid, can be used to better characterize the morphological change of estuarine islands [48].

According to Shanghai's new strategic development plans [3], in the future, land reclamation will continue to be implemented in the Hengsha East Shoal region (planned to be completed by 2019). There is still a vast expanse of beach that can be used for reclamation at the east side (approximately 370 km<sup>2</sup>) of Hengsha Island. This means that reclamation will keep occurring on Hengsha Island for a certain period in the future. Hence, continuous observations of the estuarine islands are important to track their temporal changes and assess the influence of continued human activities on the coastal environment. Changxing Island and Hengsha Island are two typical estuarine islands modified by intensive human activities. In many other coastal regions with high population densities, such satellite data and the methodology of this study can also be used to monitor the temporal changes in the estuarine islands or the coastline.

## 6. Conclusions

In this paper, the annual-scale temporal changes of two estuarine islands, which are located in Shanghai near the Yangtze River Estuary, were obtained from Landsat (TM and ETM+) data for the period of 1987–2016 based on Google Earth Engine and MATLAB. The water index and threshold segmentation methods were the main techniques used to map the estuarine islands. The temporal changes of the land area of Changxing Island and Hengsha Island were presented in a manner that comprehensively describes the variations of the two islands. The main conclusions are as follows:

1. The time series of Landsat (TM and ETM+) imagery can be used for mapping estuarine islands and tracking their temporal changes on an annual scale. The mapping results derived from the TM data and ETM+ data are in good agreement, which supports the stability of the method. These data and the described method can also be used to continuously track the temporal change of other ground features (e.g., the river, lake, and coastline features).
2. The two estuarine islands in Shanghai experienced a net increase of their land area from 183.2 km<sup>2</sup> to 280.9 km<sup>2</sup> with a change rate of 3.3 km<sup>2</sup> per year during the period of 1987–2016, and they also exhibited a certain consistency in their temporal variations. During the sub-period from 1993 to 1998, both Changxing Island and Hengsha Island exhibited a significant land shrinkage according to the Landsat observations.
3. Sharp increases in land area were observed in 2007 and 2008 for Hengsha Island and Changxing Island, respectively. According to the high-resolution images from Google Earth, human activity (i.e., the Hengsha east shoal reclamation projects and the Qingcaosha Reservoir project) plays an essential role in the rapid expansion of the estuarine islands. Compared with Landsat images, high-resolution images can provide more details from a spatial perspective.
4. From 1987 to 2016, human activity was the most important driving factor in the temporal change of estuarine islands on an annual scale ( $R^2 = 0.41$ ,  $p$ -value < 0.001). Human activities in Changxing

Island and Hengsha Island resulted in a great land expansion of 85.72 km<sup>2</sup>, accounting for 87.73% of the total land expansion of 97.71 km<sup>2</sup>. Sea level can also partly explain the change of estuarine islands ( $R^2 = 0.114$ ,  $p$ -value < 0.01). Meanwhile, sediment discharge is not a significant driving factor in the estuarine islands' change ( $R^2 = 0.045$ ,  $p$ -value = 0.76).

**Acknowledgments:** This work was supported by the National Natural Science Foundation of China (No: 41474001) and the Surveying and Mapping Basic Research Program of National Administration of Surveying, Mapping and Geoinformation (No: 13-01-05). The authors also greatly appreciate the editors and anonymous reviewers for their efforts and time spent on this paper.

**Author Contributions:** Nan Xu and Dongzhen Jia conceived and designed the experiments; Nan Xu performed the experiments and analyzed the data; Nan Xu and Dongzhen Jia wrote the manuscript; Lei Ding and Yan Wu revised the manuscript.

**Conflicts of Interest:** The authors declare no conflict of interest.

## References

1. Yang, S.L.; Milliman, J.D.; Li, P.; Xu, K. 50,000 dams later: Erosion of the Yangtze River and its delta. *Glob. Planet. Chang.* **2011**, *75*, 14–20. [[CrossRef](#)]
2. Chen, X.; Zong, Y. Coastal erosion along the Changjiang deltaic shoreline, China: History and prospective. *Estuar. Coast. Shelf Sci.* **1998**, *46*, 733–742. [[CrossRef](#)]
3. Ruan, W.; Gong, H.; Lou, F. Discussion on the new space of strategic development and function of Hengsha, Shanghai. *Eng. Sci.* **2014**, *12*, 52–58.
4. Huang, B.; Ouyang, Z.; Zheng, H.; Zhang, H.; Wang, X. Construction of an eco-island: A case study of Chongming Island, China. *Ocean Coast. Manag.* **2008**, *51*, 575–588. [[CrossRef](#)]
5. Gao, A.; Yang, S.L.; Li, G.; Li, P.; Chen, S.L. Long-term morphological evolution of a tidal island as affected by natural factors and human activities, the Yangtze Estuary. *J. Coast. Res.* **2010**, *26*, 123–131. [[CrossRef](#)]
6. Tian, B.; Wu, W.; Yang, Z.; Zhou, Y. Drivers, trends, and potential impacts of long-term coastal reclamation in China from 1985 to 2010. *Estuar. Coast. Shelf Sci.* **2016**, *170*, 83–90. [[CrossRef](#)]
7. Ma, Z.; Melville, D.S.; Liu, J.; Chen, Y.; Yang, H.; Ren, W.; Zhang, Z.; Piersma, T.; Li, B. Rethinking China's new great wall. *Science* **2014**, *346*, 912–914. [[CrossRef](#)] [[PubMed](#)]
8. Cao, W.; Wong, M.H. Current status of coastal zone issues and management in China: A review. *Environ. Int.* **2007**, *33*, 985–992. [[CrossRef](#)] [[PubMed](#)]
9. Murray, N.J.; Clemens, R.S.; Phinn, S.R.; Possingham, H.P.; Fuller, R.A. Tracking the rapid loss of tidal wetlands in the yellow sea. *Front. Ecol. Environ.* **2014**, *12*, 267–272. [[CrossRef](#)]
10. Zhang, C.; Zheng, J.; Dong, X.; Cao, K.; Zhang, J. Morphodynamic response of Xiaomiaohong tidal channel to a coastal reclamation project in Jiangsu Coast, China. International Coastal Symposium (Plymouth, England). *J. Coast. Res.* **2005**, *65*, 630–635. [[CrossRef](#)]
11. Chen, L.; Ren, C.; Zhang, B.; Li, L.; Wang, Z.; Song, K. Spatiotemporal dynamics of coastal wetlands and reclamation in the Yangtze Estuary during past 50 years (1960s–2015). *Chin. Geogr. Sci.* **2017**, 1–14. [[CrossRef](#)]
12. Dai, Z.; Liu, J.T.; Wen, W. Morphological evolution of the south passage in the Changjiang (Yangtze River) estuary, China. *Quat. Int.* **2015**, *380–381*, 314–326. [[CrossRef](#)]
13. Zhang, T.; Yang, X.; Hu, S.; Su, F. Extraction of coastline in aquaculture coast from multispectral remote sensing images: Object-based region growing integrating edge detection. *Remote Sens.* **2013**, *5*, 4470–4487. [[CrossRef](#)]
14. Liu, Y.; Wang, X.; Ling, F.; Xu, S.; Wang, C. Analysis of coastline extraction from landsat-8 OLI imagery. *Water* **2017**, *9*, 816. [[CrossRef](#)]
15. Fugura, A.A.; Billa, L.; Pradhan, B. Semi-automated procedures for shoreline extraction using single RADARSAT-1 SAR image. *Estuar. Coast. Shelf Sci.* **2011**, *95*, 395–400. [[CrossRef](#)]
16. Sekovski, I.; Stecchi, F.; Mancini, F.; Rio, L.D. Image classification methods applied to shoreline extraction on very high-resolution multispectral imagery. *Int. J. Remote Sens.* **2014**, *35*, 3556–3578. [[CrossRef](#)]
17. Maglione, P.; Parente, C.; Vallario, A. Coastline extraction using high resolution worldview-2 satellite imagery. *Eur. J. Remote Sens.* **2014**, *47*, 685–699. [[CrossRef](#)]

18. Almonacid-Caballer, J.; Sánchez-García, E.; Pardo-Pascual, J.E.; Balaguer-Beser, A.A.; Palomar-Vázquez, J. Evaluation of annual mean shoreline position deduced from landsat imagery as a mid-term coastal evolution indicator. *Mar. Geol.* **2016**, *372*, 79–88. [[CrossRef](#)]
19. Ghosh, M.K.; Kumar, L.; Roy, C. Monitoring the coastline change of hatiya island in bangladesh using remote sensing techniques. *ISPRS J. Photogramm. Remote Sens.* **2015**, *101*, 137–144. [[CrossRef](#)]
20. Rahman, A.F.; Dragoni, D.; El-Masri, B. Response of the sundarbans coastline to sea level rise and decreased sediment flow: A remote sensing assessment. *Remote Sens. Environ.* **2011**, *115*, 3121–3128. [[CrossRef](#)]
21. Ford, M. Shoreline changes interpreted from multi-temporal aerial photographs and high resolution satellite images: Wotje Atoll, Marshall Islands. *Remote Sens. Environ.* **2013**, *135*, 130–140. [[CrossRef](#)]
22. Yu, K.; Hu, C.; Muller-Karger, F.; Lu, D.; Soto, I. Shoreline changes in west-central Florida between 1987 and 2008 from Landsat observations. *Int. J. Remote Sens.* **2011**, *32*, 8299–8313. [[CrossRef](#)]
23. Zhu, Z.; Woodcock, C.E.; Olofsson, P. Continuous monitoring of forest disturbance using all available Landsat imagery. *Remote Sens. Environ.* **2012**, *122*, 75–91. [[CrossRef](#)]
24. Boak, E.H.; Turner, I.L. Shoreline Definition and Detection: A Review. *J. Coast. Res.* **2005**, *21*, 688–703. [[CrossRef](#)]
25. Sagar, S.; Roberts, D.; Bala, B.; Lymburner, L. Extracting the intertidal extent and topography of the Australian coastline from a 28 year time series of Landsat observations. *Remote Sens. Environ.* **2017**, *195*, 153–169. [[CrossRef](#)]
26. Gens, R. Remote sensing of coastlines: Detection, extraction and monitoring. *Int. J. Remote Sens.* **2010**, *31*, 1819–1836. [[CrossRef](#)]
27. Shelestov, A.; Lavreniuk, M.; Kussul, N.; Novikov, A.; Skakun, S. Exploring google earth engine platform for big data processing: Classification of multi-temporal satellite imagery for crop mapping. *Front. Earth Sci.* **2017**, *17*, 1–10. [[CrossRef](#)]
28. Dai, Z.; Liu, J.T.; Wei, W.; Chen, J. Detection of the three gorges dam influence on the Changjiang (Yangtze River) submerged delta. *Sci. Rep.* **2014**, *4*, 6600. [[CrossRef](#)] [[PubMed](#)]
29. Wu, S.; Cheng, H.; Xu, Y.J.; Li, J.; Zheng, S. Decadal changes in bathymetry of the Yangtze River estuary: Human impacts and potential saltwater intrusion. *Estuar. Coast. Shelf Sci.* **2016**, *182*, 158–169. [[CrossRef](#)]
30. Yang, H.F.; Yang, S.L.; Xu, K.H.; Wu, H.; Shi, B.W.; Zhu, Q.; Zhang, W.X.; Yang, Z. Erosion potential of the Yangtze Delta under sediment starvation and climate change. *Sci. Rep.* **2017**, *7*, 10535. [[CrossRef](#)] [[PubMed](#)]
31. Xu, H. Modification of normalised difference water index (NDWI) to enhance open water features in remotely sensed imagery. *Int. J. Remote Sens.* **2006**, *27*, 3025–3033. [[CrossRef](#)]
32. Sunder, S.; Ramsankaran, R.; Ramakrishnan, B. Inter-comparison of remote sensing sensing-based shoreline mapping techniques at different coastal stretches of India. *Environ. Monit. Assess.* **2017**, *189*, 290. [[CrossRef](#)] [[PubMed](#)]
33. Rokni, K.; Ahmad, A.; Selamat, A.; Hazini, S. Water feature extraction and change detection using multitemporal landsat imagery. *Remote Sens.* **2014**, *6*, 4173–4189. [[CrossRef](#)]
34. Wang, X. Change in area of Ebinur Lake during the 1998–2005 period. *Int. J. Remote Sens.* **2007**, *28*, 5523–5533.
35. Ling, F.; Li, W. Estimating surface water area changes using time-series Landsat data in the Qingjiang River Basin, China. *J. Appl. Remote Sens.* **2012**, *6*, 3609.
36. Du, Z.; Li, W.; Zhou, D.; Tian, L.; Ling, F.; Wang, H.; Gui, Y.; Sun, B. Analysis of landsat-8 OLI imagery for land surface water mapping. *Remote Sens. Lett.* **2014**, *5*, 672–681. [[CrossRef](#)]
37. Gong, R.; Cui, C. Investigation and analysis of beach reclamation in three islands of Chongming. *Shanghai Water* **2011**, *27*, 20–21. (In Chinese)
38. Jin, X.; He, Y.; Kirumba, G.; Hassan, Y.; Li, J. Phosphorus fractions and phosphate sorption-release characteristics of the sediment in the Yangtze River estuary reservoir. *Ecol. Eng.* **2013**, *55*, 62–66. [[CrossRef](#)]
39. Li, B.; Yan, X.X.; He, Z.F.; Chen, Y.; Zhang, J.H. Impacts of the three gorges dam on the bathymetric evolution of the Yangtze River estuary. *Chin. Sci. Bull.* **2015**, *60*, 1735–1744. (In Chinese)
40. Ying, C.; Dong, J.; Xiao, X.; Min, Z.; Bo, T.; Zhou, Y.; Li, B.; Ma, Z. Land claim and loss of tidal flats in the Yangtze Estuary. *Sci. Rep.* **2016**, *6*, 24018.
41. Wei, T.; Chen, Z.; Duan, L.; Gu, J.; Saito, Y.; Zhang, W.; Wang, Y.; Kanni, Y. Sedimentation rates in relation to sedimentary processes of the Yangtze Estuary, China. *Estuar. Coast. Shelf Sci.* **2007**, *71*, 37–46. [[CrossRef](#)]

42. Liu, J.P.; Li, A.C.; Xu, K.H.; Velozzi, D.M.; Yang, Z.S.; Milliman, J.D.; DeMaster, D.J. Sedimentary features of the Yangtze River-derived along-shelf clinoform deposit in the East China Sea. *Cont. Shelf Res.* **2006**, *26*, 2141–2156. [[CrossRef](#)]
43. Yang, S.; Ding, P.; Zhu, J.; Zhao, Q.; Mao, Z. Tidal flat morphodynamic processes of the Yangtze Estuary and their engineering implications. *China Ocean Eng.* **2000**, *14*, 307–320.
44. Yang, S.L.; Belkin, I.M.; Belkina, A.I.; Zhao, Q.Y.; Zhu, J.; Ding, P.X. Delta response to decline in sediment supply from the Yangtze River: Evidence of the recent four decades and expectations for the next half-century. *Estuar. Coast. Shelf Sci.* **2003**, *57*, 689–699. [[CrossRef](#)]
45. Niroumand-Jadidi, M.; Vitti, A. Reconstruction of river boundaries at sub-pixel resolution: Estimation and spatial allocation of water fractions. *ISPRS Int. J. Geo-Inf.* **2017**, *6*, 383. [[CrossRef](#)]
46. Foody, G.M.; Muslim, A.M.; Atkinson, P.M. Super-resolution mapping of the waterline from remotely sensed data. *Int. J. Remote Sens.* **2005**, *26*, 5381–5392. [[CrossRef](#)]
47. Dao, P.D.; Liou, Y.A.; Chou, C.W. Detection of Flood Inundation Regions with Landsat/MODIS Synthetic Data. In Proceedings of the International Symposium on Remote Sensing 2015, Tainan, Taiwan, 22–24 April 2015.
48. Gangloff, A.; Verney, R.; Doxaran, D.; Ody, A.; Estournel, C. Investigating Rhône River plume (Gulf of Lions, France) dynamics using metrics analysis from the MERIS 300m Ocean Color archive (2002–2012). *Cont. Shelf Res.* **2017**, *144*, 98–111. [[CrossRef](#)]



© 2018 by the authors. Licensee MDPI, Basel, Switzerland. This article is an open access article distributed under the terms and conditions of the Creative Commons Attribution (CC BY) license (<http://creativecommons.org/licenses/by/4.0/>).